The Mechanism of Inactivation of 3-Hydroxyanthranilate-3,4-dioxygenase by 4-Chloro-3-hydroxyanthranilate †

ARTICLE *in* BIOCHEMISTRY · JUNE 2005

Impact Factor: 3.02 · DOI: 10.1021/bi0473455 · Source: PubMed

9 AUTHORS, INCLUDING:

Yang Zhang
Chinese Academy of Meteorological Sciences
24 PUBLICATIONS **463** CITATIONS
SEE PROFILE

Aimin Liu
University of Texas at San Antonio
79 PUBLICATIONS **1,280** CITATIONS
SEE PROFILE

The Mechanism of Inactivation of 3-Hydroxyanthranilate-3,4-dioxygenase by 4-Chloro-3-hydroxyanthranilate†

Keri L. Colabroy,‡ Huili Zhai,‡ Tingfeng Li,§ Ying Ge,‡ Yang Zhang,‡ Aimin Liu,§ Steven E. Ealick,‡ Fred W. McLafferty,‡ and Tadhg P. Begley*,‡

Department of Chemistry and Chemical Biology, 120 Baker Laboratory, Cornell University, Ithaca, New York 14853, and Department of Biochemistry, University of Mississippi Medical Center, 2500 North State Street, Jackson, Mississippi 39216

Received December 17, 2004; Revised Manuscript Received March 11, 2005

ABSTRACT: 3-Hydroxyanthranilate-3,4-dioxygenase (HAD) is a non-heme Fe^{II} dependent enzyme that catalyzes the oxidative ring-opening of 3-hydroxyanthranilate to 2-amino-3-carboxymuconic semialdehyde. The enzymatic product subsequently cyclizes to quinolinate, an intermediate in the biosynthesis of nicotinamide adenine dinucleotide. Quinolinate has also been implicated in important neurological disorders. Here, we describe the mechanism by which 4-chloro-3-hydroxyanthranilate inhibits the HAD catalyzed reaction. Using overexpressed and purified bacterial HAD, we demonstrate that 4-chloro-3-hydroxyanthranilate functions as a mechanism-based inactivating agent. The inactivation results in the consumption of 2 ± 0.8 equiv of oxygen and the production of superoxide. EPR analysis of the inactivation reaction demonstrated that the inhibitor stimulated the oxidation of the active site Fe^{II} to the catalytically inactive Fe^{III} oxidation state. The inactivated enzyme can be reactivated by treatment with DTT and Fe^{II}. High resolution ESI-FTMS analysis of the inactivated enzyme demonstrated that the inhibitor did not form an adduct with the enzyme and that four conserved cysteines were oxidized to two disulfides (Cys125-Cys128 and Cys162-Cys165) during the inactivation reaction. These results are consistent with a mechanism in which the enzyme, complexed to the inhibitor and O_2, generates superoxide which subsequently dissociates, leaving the inhibitor and the oxidized iron center at the active site.

3-Hydroxyanthranilate-3,4-dioxygenase (HAD[1]) is a non-heme Fe^{II} dependent enzyme that catalyzes the oxidative ring-opening of 3-hydroxyanthranilate (**1**) to form 2-amino-3-carboxymuconic semialdehyde (**2**) (Scheme 1). This intermediate (**2**) then cyclizes to quinolinate (**3**), a precursor to the pyridine ring of nicotinamide adenine dinucleotide (*1*). Although originally believed to be a eukaryotic protein, this enzyme was recently identified in several bacteria as part of the biosynthetic pathway which converts tryptophan to quinolinate (*2*). This pathway is of interest because quinolinate selectively activates *N*-methyl-D-aspartate (NMDA) receptors, which have been implicated in neurological disorders such as stroke, epilepsy, Huntington's disease, and AIDS-related dementia (*3, 4*). In addition, elevated levels of quinolinate have been linked to Huntington's disease, hepatic encephalopathy, and the AIDS-dementia complex (*3, 5*−*7*).

Scheme 1

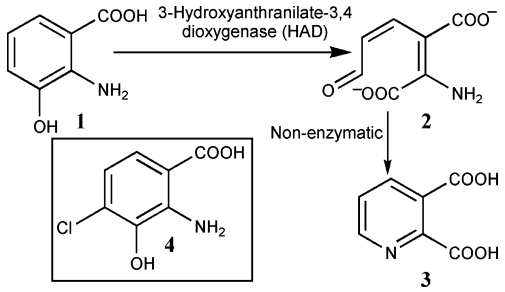

The 4-halo-hydroxyanthranilates have been previously identified as selective and potent mechanism-based inhibitors of HAD and are potentially useful drug candidates for controlling quinolinate levels (*8*−*11*). Two plausible mechanisms for this inhibition were considered based on the proposed mechanism for the closely related extradiol dioxygenases (Figure 1) (*12*−*14*). In mechanism A, the inhibitor is oxidized to the reactive acyl chloride **11**, which then acylates the enzyme. Alternatively, in mechanism B, halogen substitution could make the substrate more difficult to oxidize and therefore block the conversion of **6** to **7**, trapping the enzyme in the catalytically inactive Fe^{III} oxidation state **13**. A similar mechanism has been proposed for the inhibition of 2,3-dihydroxybiphenyl-1,2-dioxygenase by 3-chlorocatechol (*15*).

Initial studies on the inhibition of HAD by 4-chloro-3-hydroxyanthranilate (**4**) concluded that the inhibitor formed

† This work was supported by National Institutes of Health Grants DK44083 (to T.P.B.) and GM16609 (to F.W.M.).

* To whom correspondence should be addressed at the Department of Chemistry and Chemical Biology, Cornell University, Ithaca, NY 14850. Tel: (607) 255-7133. Fax: (607) 255-4137. E-mail tpb2@cornell.edu.

‡ Cornell University.

§ University of Mississippi Medical Center.

[1] Abbreviations: HAD, 3-hydroxyanthranilate-3,4-dioxygenase; ESI-FTMS, electrospray ionization Fourier transform mass spectrometry; NMDA, *N*-methyl-D-aspartate; DTT, dithiothreitol; DTNB, 5,5′-dithiobis(2-nitrobenzoic acid); CAD, collision activated dissociation; IRMPD, infrared multiphoton dissociation; ECD, electron capture dissociation; MCLA, 2-methyl-6-(4-methoxyphenyl)-3,7-dihydroimidazo[1,2-*a*]-pyrazin-3-one, hydrochloride; EPR, electron paramagnetic resonance.

10.1021/bi0473455 CCC: $30.25
Published on Web 05/03/2005

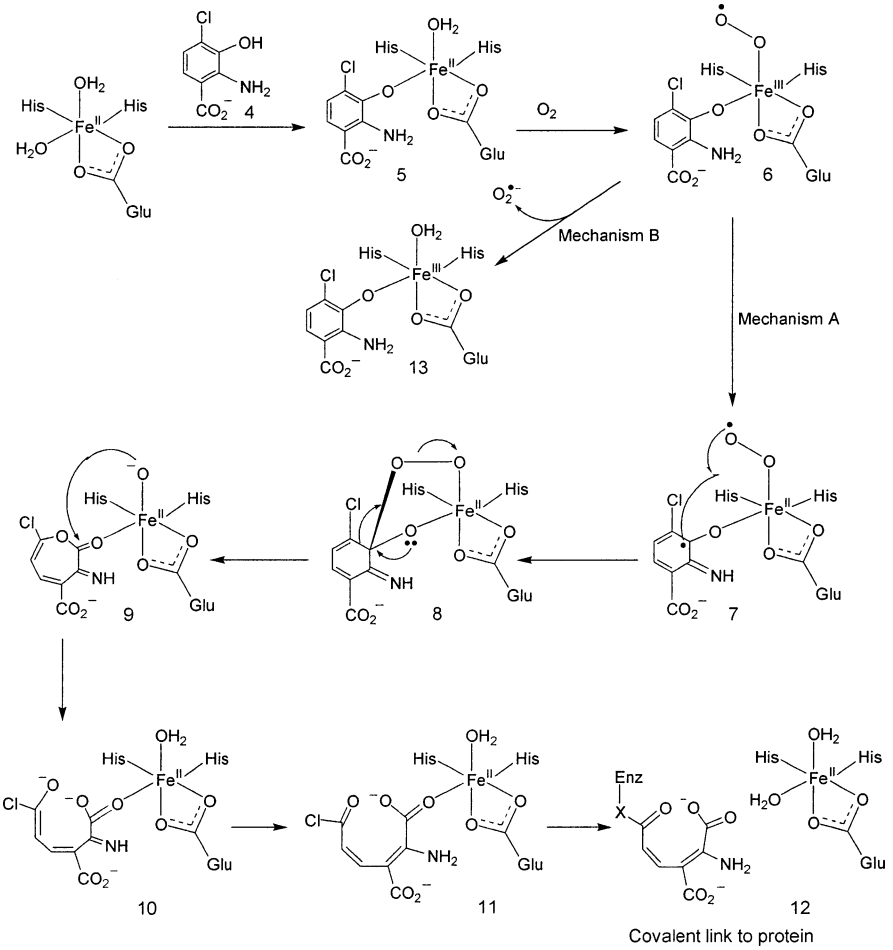

FIGURE 1: Two proposals for the mechanism of inactivation of HAD by 4-chloro-3 hydroxyanthranilate.

a covalent adduct with the enzyme (*16*). However, later studies demonstrated that inhibition was reversible at 37 °C and suggested that **4** was a tight-binding inhibitor (*10*). Detailed studies to differentiate the two possible inhibition mechanisms have not previously been possible due to the difficulty of acquiring large amounts of stable, purified HAD from eukaryotic sources (*17*−*23*). The recent discovery of the tryptophan to quinolinate pathway in a small number of bacteria has provided access to large quantities of a relatively stable HAD, now making these studies possible (*2*).

MATERIALS AND METHODS

MCLA (2-methyl-6-(4-methoxyphenyl)-3,7-dihydroimidazo[1,2-*a*]pyrazin-3-one, hydrochloride) was purchased from Molecular Probes, Inc. 4-Chloro-3-methoxybenzoic acid was purchased from Frinton Labs, Vineland, NJ. All other organic reagents were purchased from Aldrich and used without further purification. The protein concentration was determined using Coomassie Plus Protein Reagent, corrected using the extinction coefficient of HAD (ϵ = 34550 M^{-1} cm^{-1}, concentration of HAD in μM = [Coomassie concentration of HAD in μg/mL + 9.725]/35.353). Amicon Ultra-4 centrifugal filter devices were used to concentrate protein samples. Bio Spin 6 columns were purchased from Bio-Rad. UV spectra were recorded on a Hitachi U-2010 spectrophotometer. Oxygen electrode experiments were performed using a Clark polarographic oxygen probe and YSI 5300 biological oxygen monitor from Yellow Springs Instrument Co. Superoxide detection was performed using a Biolumat LB 9500 (Berthold). Kinetic data were analyzed using Origin 6.0 (Microcal Software, Inc.).

*4-Chloro-3-hydroxyanthranilate (**4**)*. **4** was synthesized from 4-chloro-3-methoxybenzoic acid as previously described (*24*).

Purification and Reconstitution of 3-Hydroxyanthranilate-3,4-dioxygenase. The HAD gene from *Ralstonia metalliduran*s was overexpressed in *Escherichia coli* Tuner (DE3) cells (Novagen) and purified by nickel affinity chromatography (Qiagen) as previously described (*2*). Purified HAD was inactive. Activity was reconstituted by incubating the inactive protein in the presence of 10 mM phosphate, 10 mM DTT, 250 mM imidazole, and 1−2 mM $FeSO_4$, at pH 8 (5−60 min). The reconstituting agents were then removed by rapid gel filtration using a Bio Spin 6 or an Econo Pac 10DG column, eluting with 10 mM phosphate buffer, pH 7.2.

3-Hydroxyanthranilate-3,4-dioxygenase Assay. The activity of HAD was monitored by measuring the absorbance increase at 360 nm resulting from the production of 2-amino-3-carboxymuconic semialdehyde as previously described (*2*) (**2**, ϵ_{360} = 47,500 M^{-1} cm^{-1}) (*18*). A typical reaction mixture consisted of 5−100 μM **1**, and 20 pmol of reconstituted HAD diluted to 500 μL with 10 mM phosphate pH 7.2 buffer.

Inhibition Kinetics. The inhibition kinetics were measured using preparations of purified, reconstituted enzyme, from which the reconstituting agents had been removed by rapid gel filtration. HAD (495 μL, 75 μM) was treated with 45 μM and 150 μM **4** (0.6 and 2.0 equiv) with stirring to

maintain an air saturated solution. Remaining activity, as a function of time, was measured by diluting 5 μL of the reaction mixture 100-fold with 10 mM phosphate pH 7.2, followed by the addition of substrate **1** (500 μM). The specific activity (μmol min^{-1} mg^{-1}) of the HAD sample, as a function of inactivation time, was determined from the rate of product formation. Activity measurements were made in triplicate. Origin 6.0 was used to analyze the data which were fit to either one ($y = A\,e^{-kt} + y_0$) or two exponential functions ($y = A_1\,e^{-k_1t} + A_2\,e^{-k_2t} + y_0$) (*25*). For the control sample, the data were fit to a single-exponential function describing the autoinactivation of HAD. For inhibitor dependent inactivation, the data were fit to two exponential functions: the first exponential function representing the rate of inactivation due to the inhibitor **4**, and the second representing the autoinactivation of HAD in buffer alone.

To determine if the inhibition was reversible, HAD (3.2 nmol) was inactivated by **4** (25 nmol) in aerated 10 mM phosphate buffer, pH 7.2, and the enzymatic activity was measured after removal of **4** by rapid gel filtration eluting with 10 mM phosphate pH 7.2.

ESI-FTMS Analysis of Inactivated HAD. Reconstituted HAD (2 mL, 133 nmol) was treated with **4**, with rapid stirring to maintain an air saturated solution. After various times (2−340 min) 200 μL of the reaction mixture was removed for MS analysis. Simultaneously 5 μL of the reaction mixture was removed and diluted 100-fold and the specific activity determined as described above.

Samples for MS analysis (200 μL) were desalted by reverse-phase protein traps (Michrom Bioresources, Auburn, CA), washed with MeOH:H_2O:AcOH (1:98:1), and eluted with MeOH:H_2O:AcOH (70:26:4). The resulting protein solution was electrosprayed at 1−50 nL/min with a nanospray emitter. The resulting ions were guided through a heated capillary, skimmer, and three radio frequency only quadrupoles into a 6 T modified Finnigan FTMS with the Odyssey data system. For MS/MS spectra, specific ions were isolated using stored waveform inverse Fourier transform (SWIFT), followed by IR multiphoton dissociation (IRMPD) (*26*), and electron capture dissociation (ECD) (*27*−*29*). MS/MS spectra were averages of 30−80 scans. Assignments of the fragment masses and compositions were made with the computer program THRASH (*30*). The mass difference (in units of 1.00235 Da) between the most abundant isotopic peak and the monoisotopic peak is denoted in italics after each reduced molecular weight (M_r) value.

Determination of the Reactive Thiol Content of HAD Using Ellman's Reagent (5,5′-Dithiobis(2-nitrobenzoic acid), DTNB). The inactivation reaction mixture consisted of reconstituted HAD (77 nmol) and **4** (100 nmol) in 600 μL of 10 mM phosphate buffer, pH 7.2, and was stirred to maintain an air saturated solution. At various time points, 50 μL of the reaction mixture was removed and diluted with 440 μL of 10 mM phosphate buffer, pH 7.2. DTNB (10 μL, 50 nmol) was added, and the 2-nitro-5-thiobenzoate anion formation was monitored at 412 nm for 2 min. An identical reaction mixture lacking **4** was analyzed as a control.

Ideal conditions for the use of DTNB in thiol titrations involve the use of deoxygenated buffers and metal chelating agents such as EDTA to prevent oxidation of free thiol to disulfide (*31*). Such conditions were not possible for HAD because the inactivation requires oxygen and EDTA could chelate the active site Fe^{II}. Therefore, the thiol titration described here, carried out in air saturated buffer containing traces of Fe^{III} from the reconstitution reaction, is likely to underestimate the accessible thiol content of the enzyme.

Superoxide Detection. MCLA (1 mg) was dissolved in 2.3 mL of argon-purged ddH_2O. The resulting solution was divided into 100 μL aliquots under argon and stored in separate tubes in the dark at −20 °C. The components of the assay mixture were added to a 3 mL cuvette in the following order: 10 mM phosphate buffer, pH 7.2 (1.92 mL), reconstituted HAD (15 nmol, 75 μL), MCLA (5 μL, freshly thawed on ice in the dark), and **4** (5 μL, 50 mM). The 465 nm luminescence was detected, in arbitrary units, using a Biolumat LB 9500. Quenching of the superoxide dependent luminescence was accomplished by adding superoxide dismutase (75 μL, 75 μg) to the assay mixture. To determine the background luminescence, an equal volume of the HAD reconstitution buffer was gel filtered and added to the reaction mixture in place of the enzyme.

*Oxygen Consumption by HAD in the Presence of Inhibitor **4**.* To generate a calibration curve for oxygen consumption, HAD (29−88 nmols, in 50 mM phosphate, 250 mM imidazole, 300 mM NaCl at pH 8) was injected into 3 mL of air saturated phosphate buffer (10mM, pH 7.2) contained in the oxygen monitor chamber in which an equilibrated oxygen electrode was submerged. Increasing concentrations of **1** were then added (50 nmol, 100 nmol, 150 nmol), and the oxygen consumption was recorded assuming that 1 mol of oxygen was consumed for each mole of substrate oxidized.

To determine if the inactivation of the enzyme by inhibitor **4** consumed oxygen, a known quantity of HAD (29−88 nmol, in 50 mM phosphate, 250 mM imidazole, 300 mM NaCl at pH 8) was injected into 3 mL of air saturated phosphate buffer (10 mM, pH 7.2) contained in the oxygen monitor chamber in which an equilibrated oxygen electrode was submerged, then a solution of inhibitor **4** in DMSO (10 μL, 1.0 μmol) was injected, and the oxygen consumption was recorded.

*Reconstitution of HAD after Inactivation by Inhibitor **4**.* Reconstituted HAD (45 μL, 2 nmol) was incubated with **4** (50 nmol, 5 μL) for 7−14 min in 10 mM phosphate buffer, pH 7.2. The inactivated enzyme was then rapidly gel filtered into 10 mM phosphate, 10 mM DTT, 250 mM imidazole pH 8 to remove the inhibitor and expose it to reducing conditions. After addition of 1−2 mM $FeSO_4$, 5 μL aliquots were removed at various time points and assayed. The control sample consisted of HAD treated in parallel under identical conditions in the absence of the inhibitor. The specific activity of the reconstituted enzyme, prior to inactivation, was 8.64 μmol min^{-1} mg^{-1}.

EPR Analyses. The samples used in the EPR analyses were reconstituted from apo-HAD with Fe^{II} under anaerobic conditions. The apoprotein was made anaerobic prior to the reconstitution by repeated cycles of evacuation and equilibration with deoxygenated argon. One molar equivalent of ferrous ion from an anaerobic $Fe(NH_4)_2(SO_4)_2$ stock solution (20 mM, argon saturated H_2O) was slowly added to the apoprotein by a gastight syringe. The 1:1 reconstituted Fe^{II}-HAD was used in the assessment of enzyme−inhibitor interactions in the presence of either $^{\bullet}NO$ or O_2 as described in the appropriate EPR experiments. EPR first derivative spectra of HAD were collected at X-band microwave

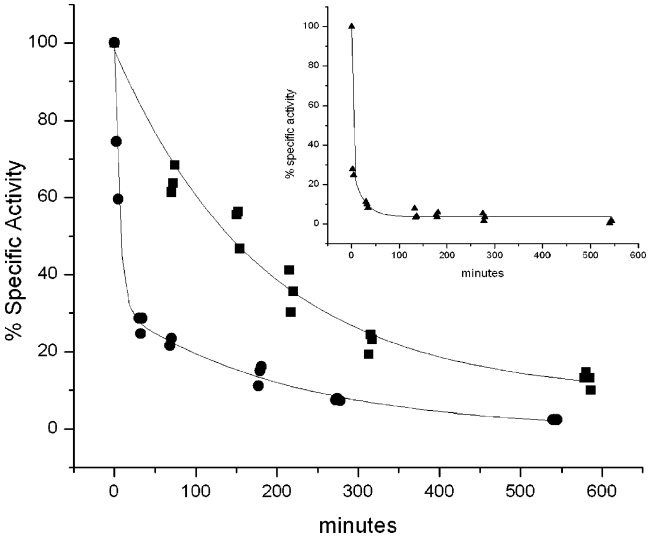

FIGURE 2: Determination of the specific activity of HAD as a function of time in the absence (■) and presence of 0.6 equivalents (●) and 2.0 equivalents (▲, inset) of inhibitor **4**.

frequency with 100 kHz field modulation using a Bruker EMX 10/12 spectrometer. The cryotemperature measurements were achieved with an Oxford Instruments ESR-900 cryostat along with LLT650/13 liquid helium transfer tube (fitted with stepper motors) and digitalized ITC503S temperature controller. Quantitative analysis was performed by double integration of the corresponding spectra and by comparison of the double integrals with each sample of identical protein concentrations recorded under the same conditions.

RESULTS

Overexpression, Purification, and Reconstitution of HAD. The HAD gene from *R. metallidurans* was overexpressed as a soluble protein in *E. coli* Tuner (DE3) cells, and purified by Ni-NTA affinity chromatography. The purified HAD was inactive, but could be reconstituted by incubation in the presence of phosphate, DTT, imidazole, and $FeSO_4$, at pH 8. The reconstituting buffer was removed by rapid gel filtration immediately preceding any assay, preventing the possibility of regenerating the active site Fe^{II} post inactivation. The specific activity (μmol min^{-1} mg^{-1}) of purified, reconstituted HAD was determined by monitoring the formation of **2** at 360 nm ($\epsilon = 47500$ M^{-1} cm^{-1}). Reconstituted HAD is only moderately stable, showed initial specific activities in the range of 8−50 μmol min^{-1} mg^{-1}, and loses activity over time with a half-life of 161 ± 11 min.

*Kinetics of HAD Inactivation by Inhibitor **4**.* The rate of inactivation of HAD by inhibitor **4** was determined by monitoring the specific activity of the inhibitor-treated enzyme over time. Samples from the inhibition reaction mixture were diluted 100-fold before activity measurement to minimize the effect of the inhibitor on the activity assay. The inactivation of HAD by **4** was so rapid that equimolar concentrations of the inhibitor produced a rate of inactivation that was too fast to measure and reliably fit using any exponential function (Figure 2, inset). In order to quantitate a lower limit for the rate of inhibitor dependent inactivation, substoichiometric concentrations of inhibitor were used. As shown in Figure 2, 0.6 equiv of **4** inactivates a fraction of the HAD population very rapidly (0.17 min^{-1} ± 0.01), and the remaining HAD loses activity at a slower rate (0.0047 min^{-1} ± 0.0008) which is consistent with the rate of autoinactivation (0.0055 min^{-1} ± 0.0006). These rates indicate that the inhibitor dependent inactivation is 35-fold faster than the autoinactivation of HAD. This rate of inactivation is an underestimate of the inactivation rate under saturating concentrations of the inhibitor, since increasing concentrations of **4** produced complete inactivation at rates which were too fast to measure. Furthermore, these rapid inactivation rates made it impossible to determine the dependence of inactivation rate on inhibitor concentration necessary to establish K_i and k_{inact} by steady state methods.

We were unable to isolate unreacted inhibitor from the inactivation reaction mixture because **4** undergoes a complex nonenzymatic oxidation in the reaction buffer.

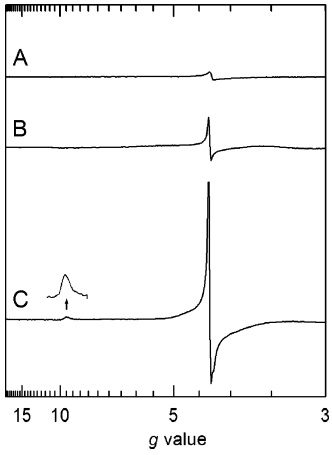

FIGURE 3: EPR spectra of HAD recorded at 5 K: (A) HAD (0.2 mM) reconstituted with 1 equiv of Fe^{II}; (B) HAD, air exposed for 30 min at room temperature; and (C) HAD (0.2 mM) incubated with 4-chloro-3-hydroxyanthranilic acid (10 equiv) in the air for 30 min. EPR parameters: microwave frequency 9.38 GHz, microwave power 1.00 mW, modulation amplitude 0.8 mT, sweep time 167 s. Inset: an enlarged $g = 9.49$ resonance for spectrum C.

EPR Analyses of Fe^{II}-Reconstituted HAD. The active form of Fe-reconstituted HAD was EPR silent, consistent with the expectation of a non-heme mononuclear Fe^{II} center with d^6 electronic configuration (Figure 3A). When the active enzyme was incubated with the inhibitor for 30 min, the EPR spectrum (trace C) presents resonances at $g = 4.25$, 4.31, and 9.49. In a control experiment, the Fe-reconstituted HAD was allowed to undergo an air exposure for 30 min at room temperature prior to the EPR measurement. The EPR spectrum of this control sample presents only the $g = 4.31$ resonance (trace B). The EPR spectrum in the inhibitor-inactivated sample is interpreted as originating from two sets of superimposed oxidized ferric EPR signals, i.e., a mixture of an $S = {}^5/_2$ ($g = 4.3$) Fe^{III} which is indistinguishable from trace B of the autoinactivated sample, and an $S = {}^5/_2$ (with resolved g components at 4.25, 4.31, and 9.49) Fe^{III} species. The Fe heterogeneity is believed due to the lack of the inhibitor at some of the enzyme active sites. The small fraction of the $g = 4.3$ signal is attributed to the autooxidation in the absence of the inhibitor. In the autooxidized sample, the Fe^{III}/HAD ratio detected was 0.12 ± 0.05 after 30 min air exposure; while in the inhibitor-inactivated sample, it was 0. 75 ± 0.05.

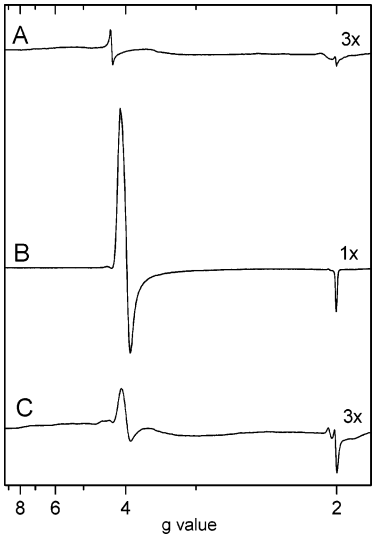

FIGURE 4: EPR spectra of the (A) HAD (0.2 mM) Fe^{II}−nitrosyl complex in the absence of substrate, **1**; (B) HAD (0.2 mM), Fe^{II}−nitrosyl complex in the presence of substrate, **1**; and (C) HAD (0.2 mM), Fe^{II}−nitrosyl complex in the presence of inhibitor, **4**. The spectra were obtained at 5 K with microwave frequency 9.38 GHz, microwave power 1.00 mW, modulation amplitude 0.3 mT, sweep time 167 s per scan. Spectra A and C were the average of three scans while spectrum B was from a single scan.

Using nitric oxide (•NO) as a spin probe and an O_2 analogue, we examined the interactions of the HAD Fe^{II} center with **1** and **4**. In the active form of the enzyme, the Fe^{II} center had very low •NO affinity. Under 5 psi of •NO pressure, almost no Fe^{II}−nitrosyl complex could be detected (Figure 4A). This EPR spectrum exhibits a weak EPR resonance at $g = 4.3$, which is assigned to an oxidized iron species in a minor fraction of the sample. In contrast, in the presence of the substrate 3-hydroxyanthraniliate, the HAD Fe^{II} center showed a substantially higher affinity for •NO. An axial EPR signal ($g = 2.00, 3.97, 4.09$) dominated this EPR spectrum (Figure 4B), typical of an $\{Fe\text{-}NO\}^7$ complex in a non-heme ligand environment as previously observed in numerous non-heme iron enzymes and model complexes (*25*, *33*−*35*). The EPR signal accounts for nearly 80% of the Fe^{II} added to the apo-HAD during reconstitution. This increased •NO affinity tends to be a general property for all of the characterized extradiol dioxygenases; substrate-binding activates the metals for subsequent O_2 (or •NO) coordination (*25*, *35*). The 4-chloro-3-hydroxyanthranilate was also shown to be capable of generating a similar iron−nitrosyl complex with •NO, but the EPR signal intensity at $g = 4.0$ is 1 order of magnitude lower than that of the substrate in the same region (Figure 4C). In this dioxygenase, neither **1** nor **4** binding causes a large splitting of the *g*-anisotropy in the low field region of the Fe−NO complexes as observed in other non-heme Fe enzymes. The order of magnitude difference in EPR signal intensity observed for the Fe−NO complexes at $g = 4.0$ may be correlated with the strength of Fe interaction with **1** and **4** as described in the accompanying paper (*50*). **4** is shown in the crystal structure to bind the Fe center in a monodentate manner using its hydroxyl group, whereas **1** binds Fe in a bidentate fashion and causes a significant change at the protein ligand set, i.e. Glu^{57} becomes monodentate in response to the HAA binding. This difference may cause a different degree of increased •NO affinity at the Fe center. Taken together, these results suggest that the inhibitor binds to the ferrous center, and more importantly, that the inactivation resulted in the conversion of the ferrous ion to the ferric oxidation state.

Analysis of Inactivated HAD by ESI-FTMS. The mass of HAD, after treatment with 5 equiv of **4**, was determined by ESI-FTMS. The mass spectrum of inactivated HAD demonstrates the absence of any covalent adduct between the inhibitor and the enzyme (Figure 5). However, the inactivated enzyme showed a mass loss of 4 Da. DTT treatment restored the 4 Da mass loss suggesting that inactivation resulted in the formation of two disulfide bonds. In a control reaction, reconstituted HAD, incubated in reaction buffer in the absence of inhibitor **4**, showed no change in mass over 340 min.

Ellman's Reagent as a Test for Disulfide Bond Formation. Ellman's reagent (5,5′-dithiobis(2-nitrobenzoic acid), DTNB) was used to measure the accessible thiol content of HAD in the presence and absence of inhibitor. The results are shown in Figure 6. In the control reaction, HAD was treated with DTNB in the absence of the inhibitor. Under these conditions, two of the five cysteines present in HAD could be detected. This value decreased over time due to air oxidation of the enzyme. For the inhibitor treated sample, the concentration of accessible cysteine decreased at a rate of 0.18 min^{-1}. This is approximately equal to the rate of enzyme inactivation with subsaturating concentrations of the inhibitor suggesting that disulfide bond formation occurs at a rate that is significantly slower than the rate of enzyme inactivation. While the absolute value of this thiol titration is likely to be an underestimate of the free thiol content of the enzyme, due to aerobic thiol oxidation in the presence of trace quantities of Fe^{III}, this experiment clearly demonstrates that the inactivation of HAD by inhibitor **4** is accompanied by disulfide bond formation in agreement with the ESI-FTMS analysis. MS analysis of the enzyme incubated in air for 340 min did not show detectable levels of the 4 Da depleted species. This is not consistent with the thiol titration of the enzyme shown in Figure 6 and suggests that the disulfide containing enzyme is selectively lost during the course of the sample preparation for MS analysis. This is also consistent with our observation of decreased yields of recovered protein when inhibitor treated HAD is prepared for analysis by mass spectrometry (see Materials and Methods).

MS/MS Analysis of Inactivated HAD. To localize the position of the two disulfides in inactivated HAD, IRMPD (*26*), SORI-CAD (*36*), and ECD (*27*−*29*) were used to dissociate the parent ion in the mass spectrometer (Figure 7). For the N-terminal poly-histidine tagged protein, 144 out of the possible 194 interresidue sites were cleaved. For the purposes of discussing the MS analysis, residue numbering will begin with the Met of the poly-histidine tag, which was added to the HAD sequence to facilitate purification. Therefore, according to this numbering scheme, the native HAD sequence begins at Met^{22} (*25*).The protein mass as well as the masses of the N-terminal fragments demonstrated that the amino terminal methionine was absent. The 4 Da mass difference is not in the N-terminal sequence because the $\boldsymbol{b_{121}}$ ion did not show the 4 Da mass loss. For the C-terminal fragments, masses of seven $\boldsymbol{y}$ and $\boldsymbol{z^{\bullet}}$ ions indicate a correct sequence prediction for the last nine residues of the C-terminus, but the $\boldsymbol{y_{13-41}}$ and $\boldsymbol{z^{\bullet}_{13-42}}$ are 1 or 2 Da lower than

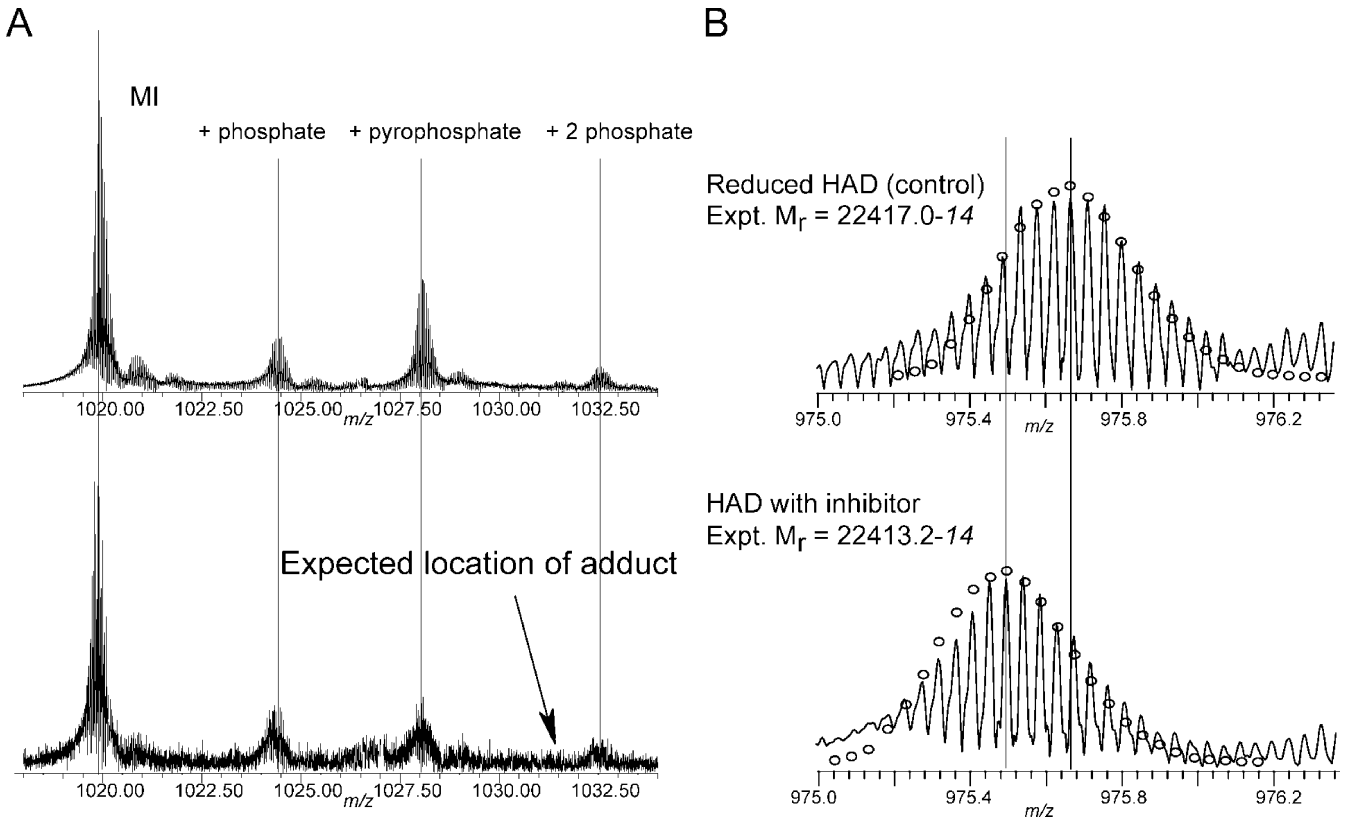

FIGURE 5: ESI-FTMS analysis of native and inhibitor treated HAD: (A) region of the mass spectrum showing the parent ion, its phosphate adducts, and the expected location of the adduct **12**; and (B) expanded view of the HAD parent ion for the native and the inactivated enzyme showing that inactivation causes a 4 Da reduction in the mass of the enzyme.

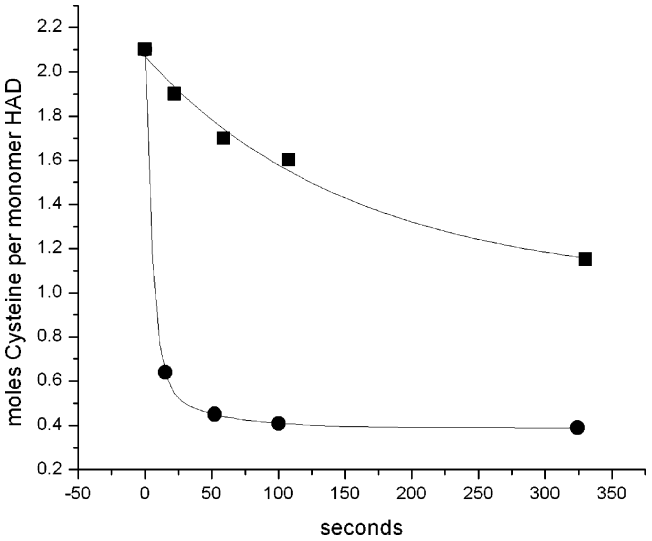

FIGURE 6: Determination of the accessible cysteine content of HAD over time in the presence (●) and absence (■) of inhibitor **4**.

the predicted mass values. This mass deficit can be explained by the formation of a disulfide bond between Cys183 and Cys186. The expected 2 Da mass deficit is not always observed in the ECD spectrum before or after the electron capture event that cleaves the protein backbone; ECD can also cleave the S−S bond to add a hydrogen atom to one of the Cys residues (*27*, *28*, *37*). The mass values of the y_{50-186} and $z^{\bullet}_{50-135}$ are lower than the sequence predicted values by even larger numbers, up to 4 Da, consistent with the formation of another disulfide bond between Cys146 and Cys149. Masses of y_{50-68} and $z^{\bullet}_{50-68}$ indicate that Cys127 is not involved in forming alternative disulfide bonds.

*Superoxide Production during HAD Inactivation by **4**.* Superoxide can be detected by its chemiluminescent reaction with MCLA which results in light emission at 465 nm (*38*). To test for superoxide production during the inactivation of HAD, the reconstituted enzyme was incubated with MCLA and inhibitor **4** and the chemiluminescence was recorded (Figure 8). Column 1 shows the signal from the inhibition reaction mixture. To confirm that this signal was due to superoxide, superoxide dismutase was added to the reaction mixture and the expected decrease in luminescence was observed (columns 2 and 4). Since Fe^{II} can also react with oxygen to produce superoxide, it was essential to measure the chemiluminescence of an identical sample of gel filtered reconstitution buffer, lacking the enzyme. This background luminescence is shown in column 3 demonstrating that approximately half of the signal in the inactivation reaction is due to the enzymatic generation of superoxide. In order to observe luminescence, very high concentrations of enzyme were used. Even under these conditions, the signal was just above background. This assay therefore does not have the sensitivity for quantitation, and we use it only as a qualitative indicator of superoxide production during inactivation.

Inhibitor Dependent Oxygen Consumption by HAD. Oxygen consumption by HAD in the presence of an excess of inhibitor **4** was measured using an oxygen electrode and determined to be 2.0 ± 0.8 nmol of oxygen for every 1 nmol of HAD. The relatively large error in this experiment is caused by poor reproducibility due to enzyme instability.

Reactivation of Inhibited HAD. It was possible to reactivate the inhibited enzyme by treating with DTT and Fe^{II} after removal of the inhibitor by gel filtration. The time course

FIGURE 7: Product ion map from MS/MS analysis of HAD treated with **4**. Residue numbering in this figure is based on the poly-histidine tagged HAD sequence and not on the gene sequence. Numbering from the N- to C-terminus is from top to bottom on the right-hand side of the figure and is used for fragments containing the N-terminus. Numbering from the C- to N-terminus is from bottom to top on the left-hand side of the figure and is used for fragments containing the C-terminus. The native HAD sequence begins at Met[22], which is underlined in red. Disulfide forming cysteines are also indicated in red. Each of the following symbols, red and blue ⎤⎣ and green *, denotes a unique cleavage of the protein. ECD induced cleavages between the nitrogen of the protein backbone amide and an adjacent α carbon generate ***c*** fragments (blue ⎤) containing the N-terminus and ***z***• fragments (blue ⎣) containing the C-terminus. CAD or IRMPD induced cleavage of an amide bond in the protein backbone generates ***b*** fragments (red ⎤) containing the N-terminus and ***y*** fragments (red ⎣) containing the C-terminus. CAD or IRMPD induced cleavages between the carbonyl carbon of a peptide bond and an adjacent α carbon generate ***a*** fragments (green *) containing the N-terminus. The mass changes for individual fragments that allowed assignment of the disulfide bonds are indicated by the following symbols: loss of 1 Da (green filled box), 2 Da (black filled box), 3 Da (green filled circle), or 4 Da (black filled circle).

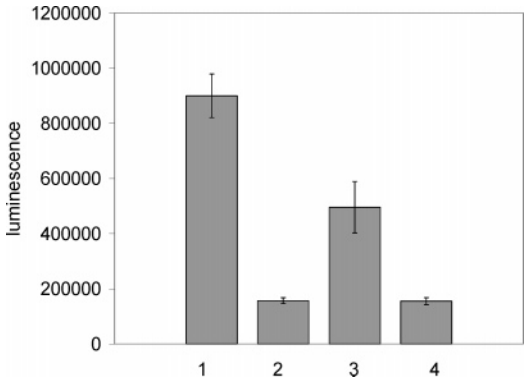

FIGURE 8: Detection of superoxide production during the inactivation of HAD by inhibitor **4** using a chemiluminescence assay. Column 1: Enzymatic reaction mixture with inhibitor **4**. Column 2: Enzymatic reaction mixture with inhibitor and superoxide dismutase. Column 3: Same as column 1 except HAD has been omitted. Column 4: Same as column 1 except HAD and the inhibitor have been omitted.

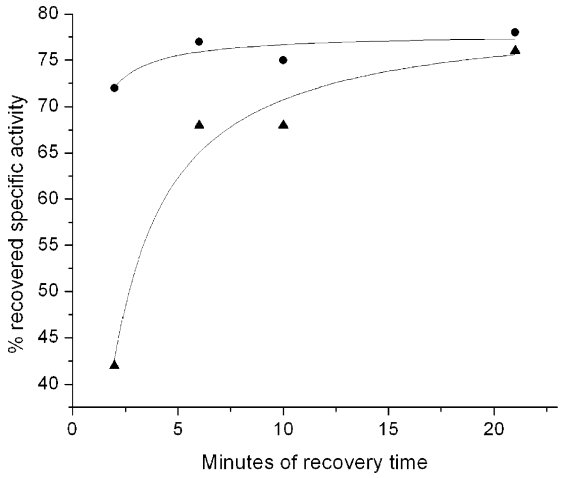

FIGURE 9: Reconstitution of HAD catalytic activity from HAD inactivated by aerobic incubation (●) and by treatment with inhibitor **4** (▲).

for this reactivation as well as for the reactivation of enzyme treated under identical conditions but in the absence of the inhibitor is shown in Figure 9. Most of the catalytic activity (75%) of the inactivated enzyme could be restored under these conditions.

DISCUSSION

The availability of highly overexpressed and relatively stable HAD from the heterologous expression of the *R. metallidurans* HAD gene in *E. coli* has enabled us to revisit the poorly characterized mechanism of inhibition of this enzyme by halogenated substrate analogues. Two mechanisms for the inactivation by 4-chloro-3-hydroxyanthranilate **4** were initially considered; one involving the acylation of the enzyme by **11** (Figure 1, mechanism A), the other involving the blocking of the electron transfer converting **6** to **7** (Figure 1, mechanism B). These two mechanisms can be readily differentiated experimentally: mechanism A predicts the formation of an acylated enzyme **12** resulting in an enzyme mass increase of 184 Da; mechanism B predicts that inhibition will be reversible under reducing conditions and will result in superoxide production (**6** to **13**) and the oxidation of the active site Fe^{II} to Fe^{III} (**5** to **6**).

MS analysis of the inactivated enzyme demonstrated unequivocally that inhibitor **4** did not form an adduct with the enzyme, eliminating mechanism A (Figure 5). The detection by EPR of Fe^{III} at the active site of the inactivated enzyme (Figure 3), the detection of superoxide production during the inactivation reaction (Figure 8), and the reactivation of the enzyme by treatment with Fe^{II}/DTT (Figure 9) are all consistent with inactivation occurring by the inhibition of electron transfer from the halogenated substrate to the active site Fe^{III} (**6** to **13** in Figure 1). In addition, the inhibited enzyme could be reactivated when the enzyme was treated with excess Fe^{II} and DTT (Figure 9). However, the MS analysis of the inactivated enzyme revealed that the inactivation mechanism is more complex than described in mechanism B because the inactivated enzyme is 4 Da lighter than the native enzyme. This mass deficit suggests that the

inactivation is accompanied by the formation of two disulfide bonds. This was further supported by demonstrating that inactivation reduced the free thiol content of the enzyme and consumed 2 mol of oxygen/mol of enzyme. In addition, DTT treatment of the inactivated enzyme restored the missing 4 Da and was required for reconstitution of activity. Finally, MS/MS analysis localized the two disulfides to Cys125-Cys128 and Cys162-Cys165 (numbering for native HAD sequence).

While our data are consistent with the trapping of intermediate **6**, it is unlikely that the trapping of this intermediate is due to the perturbation of the substrate redox potential by the chloride as previously proposed for the inactivation of 2,3-dihydroxybiphenyl-1,2-dioxygenase (*15*). While we do not have redox potentials for the substrate and inhibitor, it is likely that these potentials will be very similar because the reduction potentials of the phenoxy, the 2-chlorophenoxy, and the 4-chlorophenoxy radicals are 0.86 V, 0.93 V, and 0.85 V, respectively (*39*). In the more electron rich aminophenol substrate, we expect these perturbations to be even smaller. In addition, intermediate **6** can be regarded as a resonance form of intermediate **7**, again making it unlikely that small perturbations in the substrate redox potential are responsible for intermediate trapping. An alternative inactivation proposal is therefore needed. One possibility is that the chloro substituent perturbs the substrate binding in such a way that the addition of oxygen of the C3 carbon of the substrate is blocked. This proposal will be addressed in the accompanying paper (*50*) on the structure of the enzyme inhibitor complex.

The detection of a pair of disulfides in the inactivated enzyme was unanticipated. The cysteines involved are conserved across most bacterial and several fungal HAD sequences, suggesting that Cys125, Cys128, Cys162, and Cys165 are functionally important. A major insight into the function of these cysteines was recently obtained by solving the X-ray crystal structure of HAD (see the accompanying paper (*50*)). This structure revealed that these residues constitute the ligands for a rubredoxin-like mononuclear iron center located 24 Å from the active site of HAD. Rubredoxin is a small highly conserved protein involved in 1 electron transfer reactions (*40*, *41*). The function of this center in HAD is currently unknown. It may play a structural or a regulatory role. Alternatively, superoxide may occasionally dissociate from the enzyme during its normal catalytic cycle, generating the inactive Fe^{III} enzyme, which is then reactivated by long range (24 Å) electron transfer from the reduced rubredoxin site. In some respects, HAD is analogous to the superoxide reductase−rubredoxin system for superoxide detoxification in anaerobic bacteria (*42*−*47*). Superoxide reductases from several organisms have been characterized, and two families have been identified. The mononuclear superoxide reductases contain a single Fe^{II} at the active site and use a separate rubredoxin as the reducing agent. The binuclear superoxide reductase contains the same active site Fe^{II} and is fused to a rubredoxin domain. A characterized example of the binuclear superoxide reductase from *Desulfovibrio desulfuricans* has the rubredoxin site located 22 Å from the active site Fe^{II} (*45*). Superoxide mediated electron transfer has been demonstrated between the *Treponema pallidum* mononuclear superoxide reductase and its physiological rubredoxin (*48*); however, there is as yet no experimental evidence for superoxide mediated electron transfer between the catalytic Fe^{II} and the fused rubredoxin domain of a binuclear superoxide reductase. Interestingly, binding of ferrocyanide to the active site of the *Desulfovibrio vulgaris* binuclear superoxide reductase also resulted in demetalation and oxidation of the rubredoxin site (*49*). While the similarities between HAD and superoxide reductase/rubredoxin suggest that the rubredoxin site on HAD plays an electron transfer role, the possibility that this site functions as an independent catalytic domain or plays a structural or regulatory role cannot yet be ruled out.

ACKNOWLEDGMENT

We thank Jennie Sanders for determining the extinction coefficient of HAD, and for help with analysis of kinetic data.

REFERENCES

1. Colabroy, K. L., and Begley, T. P. (2005) The Pyridine Ring of NAD Is Formed by a Nonenzymatic Pericyclic Reaction, *J. Am. Chem. Soc. 127*, 840−841.
2. Kurnasov, O., Goral, V., Colabroy, K., Gerdes, S., Anantha, S., Osterman, A., and Begley, T. P. (2003) NAD biosynthesis: Identification of the tryptophan to quinolinate pathway in bacteria, *Chem. Biol. 10*, 1195−1204.
3. Stone, T. W., and Darlington, G. L. (2002) Endogenous kynurenines as targets for drug discovery and development, *Nat. Rev. Drug Discovery 1*, 609−620.
4. Schwarcz, R. (2004) The kynurenine pathway of tryptophan degradation as a drug target, *Curr. Opin. Pharmacol. 4*, 12−17.
5. Achim, C., Heyes, M., and Wiley, C. (1993) Quantitation of Human Immunodeficiency Virus, Immune Activation Factors, and Quinolinic Acid in AIDS Brains, *J. Clin. Invest. 91*, 2769−2775.
6. Schwarcz, R., Okuno, E., White, R. J., Bird, E. D., and Whetsell, W. O., Jr. (1988) 3-Hydroxyanthranilate oxygenase activity is increased in the brains of Huntington disease victims, *Proc. Natl. Acad. Sci. U.S.A. 85*, 4079−4081.
7. Heyes, M. (1993) Metabolism and neuropathologic significance of quinolinic acid and kynurenic acid, *Biochem. Soc. Trans. 21*, 83−89.
8. Heyes, M., Hutto, B., and Markey, S. (1988) 4-Chloro-3-Hydroxyanthranilate Inhibits Brain 3-Hydroxyanthranilate Oxidase, *Neurochem. Int. 13*, 405−408.
9. Saito, K., Chen, C., Masana, M., Crowley, J., Markey, S., and Heyes, M. (1993) 4-Chloro-3-hydroxyanthranilate, 6-chroro-tryptophan and norharmane attenuate quinolinic acid formation by interferon-y-stimulated monocytes (THP-1-cells), *Res. Commun.*, 12−14.
10. Walsh, J., Todd, W., Carpenter, B., and Schwarcz, R. (1991) 4-Halo-3-Hydroxyanthranilic Acids: Potent Competitive Inhibitors of 3-Hydroxy-Anthranilic Acid Oxygenase in Vitro, *Biochem. Pharmacol. 42*, 985−990.
11. Walsh, J., Todd, W., Carpenter, B., and Schwarcz, R. (1991) 4-Halo-3-Hydroxyanthranilates are Potent Inhibitors of 3-Hydroxyanthranilate Oxygenase in the Rat Brain in Vitro and in Vivo, *Adv. Exp. Med. Biol. 294*, 579−582.
12. Bugg, T. D. H., and Lin, G. (2001) Solving the riddle of the intradiol and extradiol catechol dioxygenases: how do enzymes control hydroperoxide rearrangements, *Chem. Commun.* 941−952.
13. Lin, G., Reid, G., and Bugg, T. D. H. (2001) Extradiol Oxidative Cleavage of Catechols by Ferrous and Ferric Complexes of 1,4,7-Triazacyclononane: Insight into the Mechanism of the Extradiol Catechol Dioxygenases, *J. Am. Chem. Soc. 123*, 5030−5039.
14. Bugg, T. D. H., and Winfield, C. (1998) Enzymic cleavage of aromatic rings: mechanistic aspects of the catechol dioxygenases and later enzymes of bacterial oxidative cleavage pathways, *Nat. Prod. Rep. 15*, 513−530.
15. Vaillancourt, F., Labbe, G., Drouin, N., Fortin, P., and Eltis, L. (2002) The mechanism-based inactivation of 2,3-dihydroxybiphenyl 1,2-dioxygenase by catecholic substrates, *J. Biol. Chem. 277*, 2019−2027.
16. Parli, J. C., Krieter, P., and Schmidt, B. (1980) Metabolism of 6-chlorotryptophan to 4-chloro-3-hydroxyanthranilic acid: A

potent inhibitor of 3-hydroxyanthranilic acid oxidase, *Arch. Biochem. Biophys. 203*, 161−166.
17. Calderone, V., Trabucco, M., Menin, V., Negro, A., and Zanotti, G. (2002) Cloning of human 3-hydroxyanthranilic acid dioxygenase in Escherichia coli: characterisation of the purified enzyme and its in vitro inhibition by Zn2+, *Biochim. Biophys. Acta 1596*, 283−292.
18. Koontz, W., and Shiman, R. (1976) Beef Kidney 3-Hydroxyanthranilic Acid Oxygenase, *J. Biol. Chem. 251*, 368−377.
19. Kucharczyk, R., Zagulski, M., Rytka, J., and Herbert, C. (1998) The yeast gene YJR025c encodes a 3-hydroxyanthranilic acid dioxygenase and is involved in nicotinic acid biosynthesis, *FEBS Lett. 424*, 127−130.
20. Malherbe, P., Kohler, C., Da Prada, M., Lang, G., Kiefer, V., Schwarcz, R., Lahm, H., and Cesura, A. (1994) Molecular Cloning and Functional Expression of Human 3-Hydroxyanthranilic-acid Dioxygenase, *J. Biol. Chem. 269*, 13792−13797.
21. Okuno, E., Kohler, C., and Schwarcz, R. (1987) Rat 3-hydroxyanthranilic Acid Oxygenase: Purification from the Liver and Immunocytochemical Localization in the Brain, *J. Neurochem. 49*, 771−780.
22. Stevens, C., and Henderson, L. (1959) Beef Liver 3-Hydroxyanthranilic Acid Oxidase, *J. Biol. Chem. 234*, 1188−1190.
23. Nandi, D., Lightcap, E. S., Koo, Y. K., Lu, X., Quancard, J., and Silverman, R. B. (2003) Purification and inactivation of 3-hydroxyanthranilic acid 3,4-dioxygenase from beef liver, *Int. J. Biochem. Cell Biol. 35*, 1085−1097.
24. Melikian, A., Boigegrain, R., Kan, J., and Soubrie, P. (1990) Regioselective synthesis of 4-chloro-3-hydroxyanthranilic acid, a potent in vitro inhibitor of 3-hydroxyanthranilic acid oxygenase activity from rate brain, *Eur. J. Med Chem. 25*, 267−270.
25. Arciero, D. M., and Lipscomb, J. D. (1986) Binding of oxygen-17-labeled substrate and inhibitors to protocatechuate 4,5-dioxygenase-nitrosyl complex. Evidence for direct substrate binding to the active site iron(2+) of extradiol dioxygenases, *J. Biol. Chem. 261*, 2170−2178.
26. Little, D. P., Speir, J. P., Senko, M. W., O'Connor, P. B., and McLafferty, F. W. (1994) Infrared Multiphoton Dissociation of Large Multiply Charged Ions for Biomolecule Sequencing, *Anal. Chem. 66*, 2809−2815.
27. Sze, S. K., Ge, Y., Oh, H., and McLafferty, F. W. (2003) Plasma Electron Capture Dissociation for the Characterization of Large Proteins by Top Down Mass Spectrometry, *Anal. Chem. 75*, 1559−1603.
28. Zubarev, R. A., Kruger, N. A., Fridriksson, E. K., Lewis, M. A., Horn, D. M., Carpenter, B. K., and McLafferty, F. W. (1999) Electron Capture Dissociation of Gaseous Multiply-Charged Proteins is Favored at Disulfide Bonds and Other Sites of High Hydrogen Atom Affinity, *J. Am. Chem. Soc. 121*, 2857−2862.
29. Zubarev, R. A., Horn, D. M., Fridriksson, E. K., Kelleher, N. L., Kruger, N. A., Lewis, M. A., Carpenter, B. K., and McLafferty, F. W. (2000) Electron Capture Dissociation for Structural Characterization of Multiply Charged Protein Cations, *Anal. Chem. 72*, 563−573.
30. Horn, D. M., Zubarev, R. A., and McLafferty, F. W. (2000) Automated reduction and interpretation of high-resolution electrospray mass spectra of large molecules, *J. Am. Soc. Mass Spectrom. 11*, 320−332.
31. Riddles, P. W., Blakely, R. L., and Zerner, B. (1983) [8] Reassesment of Ellman's Reagent, *Methods Enzymol. 91*, 49−61.
32. Binnemans, K., Galyametdinov, Y. G., Deun, R. V., Bruce, D. W., Collinson, S. R., Polishchuk, A. P., Bikchantaev, I., Haase, W., Prosvirin, A. V., Tinchurina, L., Litvinov, I., Gubajdullin, A., Rakhmatullin, A., Uytterhoeven, K., and Meervelt, L. V. (2000) Rare-Earth-Containing Magnetic Liquid Crystals, *J. Am. Chem. Soc. 122*, 4335−4344.
33. Rodriguez, J. H., Xia, Y.-M., and Debrunner, P. G. (1999) Mössbauer Spectroscopy of the Spin Coupled $Fe^{2+}-\{FeNO\}^7$ Centers of Nitrosyl Derivatives of Deoxy Hemerythrin and Density Functional Theory of the $\{FeNO\}^7(S = {}^3/_2)$ Motif, *J. Am. Chem. Soc. 121*, 7846−7863.
34. Zhang, Y., Pavlosky, M. A., Brown, C. A., Westre, T. E., Hedman, B., Hodgson, K. O., and Solomon, E. I. (1992) Spectroscopic and theoretical description of the electronic structure of the $S = {}^3/_2$ nitrosyl complex of non-heme iron enzymes *J. Am. Chem. Soc. 114*, 9189−9191.
35. Davis, M. I., Wasinger, E. C., Decker, A., Pau, M. Y. M., Vaillancourt, F. H., Bolin, J. T., Eltis, L. D., Hedman, B., Hodgson, K. O., and Solomon, E. I. (2003) Spectroscopic and Electronic Structure Studies of 2,3-Dihydroxybiphenyl 1,2-Dioxygenase: O_2 Reactivity of the Non-Heme Ferrous Site in Extradiol Dioxygenases, *J. Am. Chem. Soc. 125*, 11214−11227.
36. Senko, M. W., Speir, J. P., and McLafferty, F. W. (1994) Collisional Activation of Large Multiply Charged Ions Using Fourier Transform Mass Spectrometry, *Anal. Chem. 66*, 2801−2808.
37. Ge, Y., Lawhorn, B. G., ElNaggar, M., Strauss, E., Park, J.-H., Begley, T. P., and McLafferty, F. W. (2002) Top down characterization of larger proteins (45 kDa) by electron capture dissociation mass spectrometry, *J. Am. Chem. Soc. 124*, 672−678.
38. Nakano, M. (1990) Determination of Superoxide Radical and Singlet Oxygen Bases on Chemiluminescence of Luciferin analogs, *Methods Enzymol. 186*, 585−591.
39. Li, C., and Hoffman, M. Z. (1999) One-Electron Redox Potentials of Phenols in Aqueous Solution, *J. Phys. Chem. B 103*, 6653−6656.
40. Lovenberg, W., and Sobel, B. E. (1965) Rubredoxin: A new electron transfer protein from Clostridium pasteurianum, *Proc. Natl. Acad. Sci. U.S.A. 54*, 193−199.
41. Im, S.-C., and Sykes, G. A. (1996) Kinetic Studies on the redox reactions of Clostridium pasteurianum Rubredoxin, *J. Chem. Soc., Dalton Trans. 11*, 2219−2222.
42. Coulter, E. D., and Kurtz, D. M., Jr. (2001) A Role for Rubredoxin in Oxidative Stress Protection in Desulfovibrio vulgaris: Catalytic Electron Transfer to Rubrerythrin and Two-Iron Superoxide Reductase, *Arch. Biochem. Biophys. 394*, 76−86.
43. Jenney, F. E., Jr., Verhagen, M. F., Cui, X., and Adams, M. W. (1999) Anaerobic microbes: oxygen detoxification without superoxide dismutase. *Science 286*, 306−309.
44. Yeh, A. P., Hu, Y., Jenney, F. E., Jr., Adams, M. W. W., and Rees, D. C. (2000) Structures of the superoxide reductase from Pyrococcus furiosus in the oxidized and reduced states, *Biochemistry 39*, 2499−2508.
45. Coelho, A. V., Matias, P., Fulop, V., Thompson, A., Gonzalez, A., and Carrondo, M. A. (1997) Desulfoferrodoxin structure determined by MAD phasing and refinement to 1.9-Å resolution reveals a unique combination of a tetrahedral FeS_4 center with a square pyramidal $FeSN_4$ center, *J. Biol. Inorg. Chem. 2*, 680−689.
46. Moura, I., Tavares, P., Moura, J. J. G., Ravi, N., Hanh, H. B., Liu, M. Y., and LeGall, J. (1990) Purification and characterization of desulfoferrodoxin. A novel protein from Desulfovibrio desulfuricans (ATCC 27774) and from Desulfovibrio vulgaris (strain Hildenborough) that contains a distorted rubredoxin center and a mononuclear ferrous center, *J. Biol. Chem. 265*, 21596−21602.
47. Kurtz, D. M., Jr. (2004) Microbial Detoxification of Superoxide: The Non-Heme Iron Reductive Paradigm for Combating Oxidative Stress, *Acc. Chem. Res. 37*, 902−908.
48. Auchere, F., Sikkink, R., Cordas, C., Raleiras, P., Tavares, P., Moura, I., and Moura, J. J. G. (2004) Overexpression and purification of Treponema pallidum rubredoxin; kinetic evidence for a superoxide-mediated electron transfer with the superoxide reductase neelaredoxin, *J. Biol. Inorg. Chem. 9*, 839−849.
49. Adam, V., Royant, A., Niviere, V., Molina-Heredia, F. P., and Bourgeois, D. (2004) Structure of Superoxide Reductase Bound to Ferrocyanide and Active Site Expansion upon X-Ray-Induced Photo-Reduction, *Structure 12*, 1729−1740.
50. Zhang, Y., Colabroy, K. L., Begley, T. P., and Ealick, S. E. (2005) Structural Studies on 3-Hydroxyanthranilate-3,4-dioxygenase: The Catalytic Mechanism of Complex Oxidation Involved in NAD Biosynthesis, *Biochemistry 44*, 7632−7643|

BI0473455